J Fluoresc (2013) 23:439–450
DOI 10.1007/s10895-013-1160-7

ORIGINAL PAPER

Influences of Doping and Annealing on the Structural and Photoluminescence Properties of Y_2O_3 Nanophosphors

S. Som · S. K. Sharma · T Shripathi

Received: 30 May 2012 / Accepted: 7 January 2013 / Published online: 18 January 2013

Abstract This paper reports the structural and optical properties of rare earth doped and codoped yttrium oxide nanophosphors. Dysprosium (Dy^{3+}) and Terbium (Tb^{3+}) doped and codoped yttrium oxide (Y_2O_3) phosphors were prepared by combustion synthesis method and subsequently annealed to high temperature to eliminate the hydroxyl group (−OH) and to get more crystallinity. The formation of compounds was confirmed by the X-ray diffraction (XRD), Fourier Transform Infrared Spectroscopy (FTIR). The diffuse reflectance spectra (DRS) of doped and codoped Y_2O_3 powder phosphors were measured and it is observed that the absorption edge of the doped samples is shifted towards blue region with respect to undoped sample. The bandgap of the prepared samples were evaluated with the help of Kubelka-Munk function using Diffuse Reflectance Spectra (DRS) and an increase in bandgap was observed with the decrease in crystallite size. A strong characteristics emission from Tb^{3+} and Dy^{3+} ions was identified and the influence of doping concentration and annealing temperature on photoluminescence properties was systematically studied. Transfer of energy was observed in dysprosium–terbium codoped Y_2O_3 nanophosphor at room temperature from Dy^{3+} ions toTb^{3+} ions.

Keywords Nanophosphor · XRD · Bandgap · Photoluminescence · Energy transfer

Research Highlights • This Paper discusses the effect of doping concentration and annealing temperature on the structural and photoluminescence properties of yttrium oxide phosphor.
• Structural parameters and Band gap are calculated.
• Enhancement of Tb^{3+} emission by energy transfer from Dy^{3+} is observed.

S. Som (✉) · S. K. Sharma
Department of Applied Physics, Indian School of Mines, Dhanbad 826004, India
e-mail: sudipta.som@gmail.com

T. Shripathi
UGC DAE consortium for Scientific Research, Indore 452001, India

Introduction

The synthesis and characterization of nanophosphors have attracted much attention in recent years because of their excellent luminescent properties in display and lightning devices. Compared to bulk materials, nanocrystals exhibit new and enhanced optical, electronic and structural properties due to perturbations of the electronic distribution induced by reduced dimensionality [1, 2]. Significant attention has been paid to rare earth ions doped nanomaterials to find out their potential applications in today's display technology in the photonic and optoelectronic fields. The luminescence properties of rare earth doped inorganic phosphors have been extensively investigated for potential applications in flat panel displays, plasma display panels, fluorescent lamps and white LEDs [3].

Y_2O_3 is an advanced ceramic due to its stable physical and chemical properties, which has been widely used as a host material in various luminescence applications. It also presents the advantages of highly saturated colour, which makes it a promising material for different industrial applications. Y_2O_3 is the best host for the rare earth ions, because of the similarities in the chemical properties and ionic radii of the rare earths. The Y_2O_3 is a rare earth sesquioxide and posses high melting point (2,400 °C), high thermal conductivity, wide transparency range (0.2–8 μm), wide band gap (5.6 eV), high refractive

index (~1.8) and low cut off phonon energy (380 cm^{-1}), making it a very promising host material for the production of efficient luminescent media [4]. Rare earth doped Y_2O_3 has excellent luminescence properties, such as narrow emission lines and long luminescence life time. These properties are essential for the actual applications in solar cells, display devices and optical communications. Unfortunately, rare earth ions have very small absorption cross-section of the order of $10^{-21} cm^2$, which lead to the low emission efficiency. So, codoping with another rare earth ion is an effective way to improve its luminescence intensity [5].

Trivalent terbium (Tb^{3+}) and dysprosium ion (Dy^{3+}) has been extensively studied in various hosts due to their unique spectral properties [6–8]. Meng et al. [9] reported the influence of size confinement on the energy transfer between Tb^{3+} ions in Y_2O_3 nanopowders. Nash et al. [10] demonstrated in-depth spectroscopic analysis and energy level modeling of Nd^{3+} in Y_2O_3 nanocrystals in polymeric hosts. Xin-Yuan Sun et al. [5] studied the energy transfer between Dy^{3+} and Tb^{3+}in silicate glasses. But there is no detailed study carried out on the doping and annealing effects on the structural and optical properties of Dy^{3+} and Tb^{3+} activated and coactivated Y_2O_3 nanophosphors prepared by combustion synthesis method. These studies will help to check the suitability of these phosphors in different display devices. Also, the calculation of bandgap of prepared phosphors was performed first time from diffuse reflectance spectra using Kubelka-Munk function [11].

Experimental

Dy doped, Tb doped and Tb,Dy codoped Y_2O_3 phosphors were prepared by combustion synthesis method using dysprosium oxide (Dy_2O_3), terbium oxide (Tb_4O_7), yttrium oxide (Y_2O_3), nitric acid (HNO_3) and urea ($CO(NH_2)_2$) as starting raw materials. The stock solutions of $Y(NO_3)_3$, $Dy(NO_3)_3$ and $Tb(NO_3)_3$ were prepared by dissolving Y_2O_3, $Dy_2O_3$and Tb_4O_7 in nitric acid and diluting with deionized water. The nitrate solutions were mixed according to the formula $(Y_{1-x-y}RE_xRE_y)_2\ O_3$ in a beaker and then a suitable amount of urea was added to it keeping urea to metal nitrate molar ratio as 2.5 for all the cases [12]. The mixture was then dissolved properly to achieve a uniform solution and dried by heating at 80 °C using magnetic stirrer. Finally the solid residue was transferred to silica crucible and annealed at 600 °C in a furnace for an hour. The synthesis reaction is [12]

$$(2-2x)Y(NO_3)_3 + 2xRE(NO_3)_3 + 5(NH_2)_2CO \rightarrow (Y_{1-x}RE_x)_2O_3 + 5CO_2 + 8N_2 + 10H_2O.$$

XRD spectrum of the prepared compounds were recorded in a wide range of Bragg angle 2θ (15°≤2θ ≤85°) using Bruker D8 advanced XRD with Cu target radiation (λ= 0.154056 nm). The FT-IR spectra were studied in the wavelength range 4,000–400 cm^{-1} using Perkin Elmer make FTIR-2000 Spectrometer. The Diffuse reflectance (DR) spectra were studied using PerkinElmer make Lambda-950, UV–VIS-NIR Spectrophotometer in the wavelength range 200–800 nm. The Photoluminescence (PL) studies were carried out on Hitachi make Fluorescence Spectrometer F-2500.

Results and Discussions

Structural Analysis

XRD

In order to confirm the formation of doped and codoped Y_2O_3 compounds, XRD pattern for each compound were recorded along with the commercial undoped Y_2O_3 powders (Fig. 1a). The sharp and single diffraction peaks of the XRD pattern confirm the formation of single phase compound. The doped Y_2O_3 compounds exhibit the body centered cubic structure with the space group Ia3. The (hkl) values of most prominent peaks are shown in the XRD pattern. The lattice parameters of the unit cell were a=b=c=10.60 Å with $\alpha=\beta=\gamma=90°$ which was in correspondence with the JCPDS database of pdf number 83–0927 as shown in the Fig. 1. The peak at 2θ=~29.5° was observed as the strongest peak corresponding to the plane (222) for all the compounds and no peaks were observed due to impurities. The ionic radii of Y^{3+} (0.9 Å), Dy^{3+} (0.91 Å), Tb^{3+} (0.923 Å) are very close, and hence it is possible to substitute Y^{3+} with Dy^{3+} or Tb^{3+} ions. The results show that the incorporation of Dy^{3+}, Tb^{3+} into the Y_2O_3 lattice do not influence the crystal structure.

The XRD spectrum was also recorded for the Tb^{3+} doped, Dy^{3+} doped and Tb^{3+}/Dy^{3+} codoped Y_2O_3 phosphors annealed at various temperatures (Fig. 1b–d). The phosphors annealed at 1,000 °C shows prominent diffraction peaks (2θ=~40°) which were not clearly observed in case of other annealed phosphors indicating the occurrence of crystal growth phenomena during heat treatment. Moreover, the crystallinity of the samples enhanced significantly after being annealed at high temperatures >700 °C. This shows that the crystallinity of RE^{3+} doped and codoped Y_2O_3 phase improves. The crystallite size of annealed phosphors was calculated by Debye-Scherrer formula (Eq. 1) indicating an increase in crystallite size for the phosphors annealed from 500 °C to 1,000 °C temperatures.

Structural Parameters

The structural parameters such as crystallite size (D), strain (ε), particle density (D_x) and dislocation density (δ)

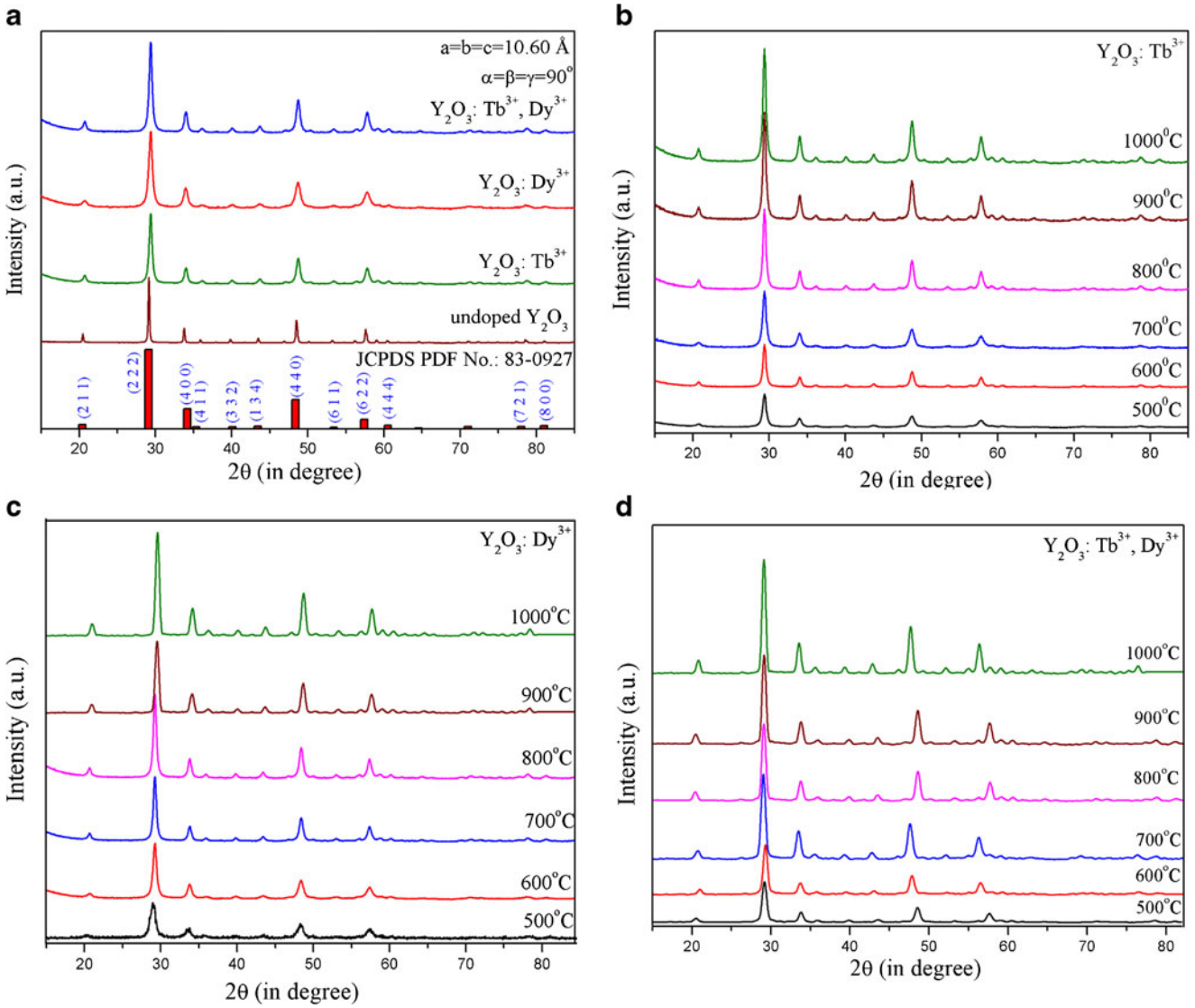

Fig. 1 XRD spectra of the prepared samples for different dopants (**a**) and annealing temperature (**b**–**d**)

associated with the doped and codoped phosphors were calculated from the XRD data. The crystallite size was determined from Debye-Scherrer equation [13]

$$D = 0.9\lambda/\beta\cos\theta \quad (1)$$

Here λ is the wavelength of the X-rays (1.54056 Å), β is the full-width at half maximum (FWHM) and θ is the angle of diffraction. The estimated crystallite size of doped and codoped Y_2O_3 phosphors is summarized in Table 1.

The peak broadening in prepared phosphors arises not only due to crystallite size but also may be due to strain present. Strain and crystallite size effects in peak broadening are independent to each other and they can be distinguished by Hall-Williamson plot. The Hall-Williamson relation [13] expresses the FWHMs (β) as a linear combination of the contributions from the strain (ε) and crystallite size (D):

$$\beta\cos\theta/\lambda = 1/D + \varepsilon\sin\theta/\lambda \quad (2)$$

Figure 2 shows the plot of βcosθ/λ versus sinθ/λ for doped and codoped Y_2O_3, which is a straight line. The reciprocal of intercept of this line on the βcosθ/λ axis gave the average crystallite size (D). The crystallite size for the various phosphors calculated by Hall-Williamson plot is summarized in Table 1. The results were in agreement with the Debye-Scherrer formula. The strain value (ε) was obtained from the slope of the line and comes out to be very small ~10^{-3}, which implies the negligible effect of strain in XRD broadening.

Table 1 Structural parameters of doped and codoped Y_2O_3 phosphors

Material	Maximum Peak (2θ) (deg.)	FWHM (β) (deg.)	lattice parameter a (Å)	Crystallite size D (nm)		Particle density (D_x) gm/cm^3	dislocation density (δ)(×10^{15}/m^2)	Microstrain (ε) (× 10^{-3})
				Debye Sherrer	Hall Williamson			
Y_2O_3: Dy^{3+}	29.39	0.3812	10.60	10–20	20	5.0365	2.5	0.77
Y_2O_3: Tb^{3+}	29.40	0.3812	10.60	10–60	40	5.0365	2.23	5.49
Y_2O_3: Dy^{3+}, Tb^{3+}	29.45	0.3226	10.60	10–60	35	5.0365	1.6	3.89
Undoped Y_2O_3	29.11	0.157	10.60	60–120	60	5.0365	0.37	1.52

The particle density (D_x) and dislocation density (δ) were calculated from the formulae [14, 15]:

$$D_x = 16M/(Na^3) \quad (3)$$

$$\delta = 1/D^2 \quad (4)$$

where M is the molecular mass, N is the Avogadro's number and a, is the lattice parameter. The values of particle density and dislocation density are summarized in Table 1.

FTIR

The FT-IR spectra of the prepared doped, codoped and commercial undoped Y_2O_3 phosphors are shown in Fig. 3a. The absorption band centered at 560 cm^{-1} is

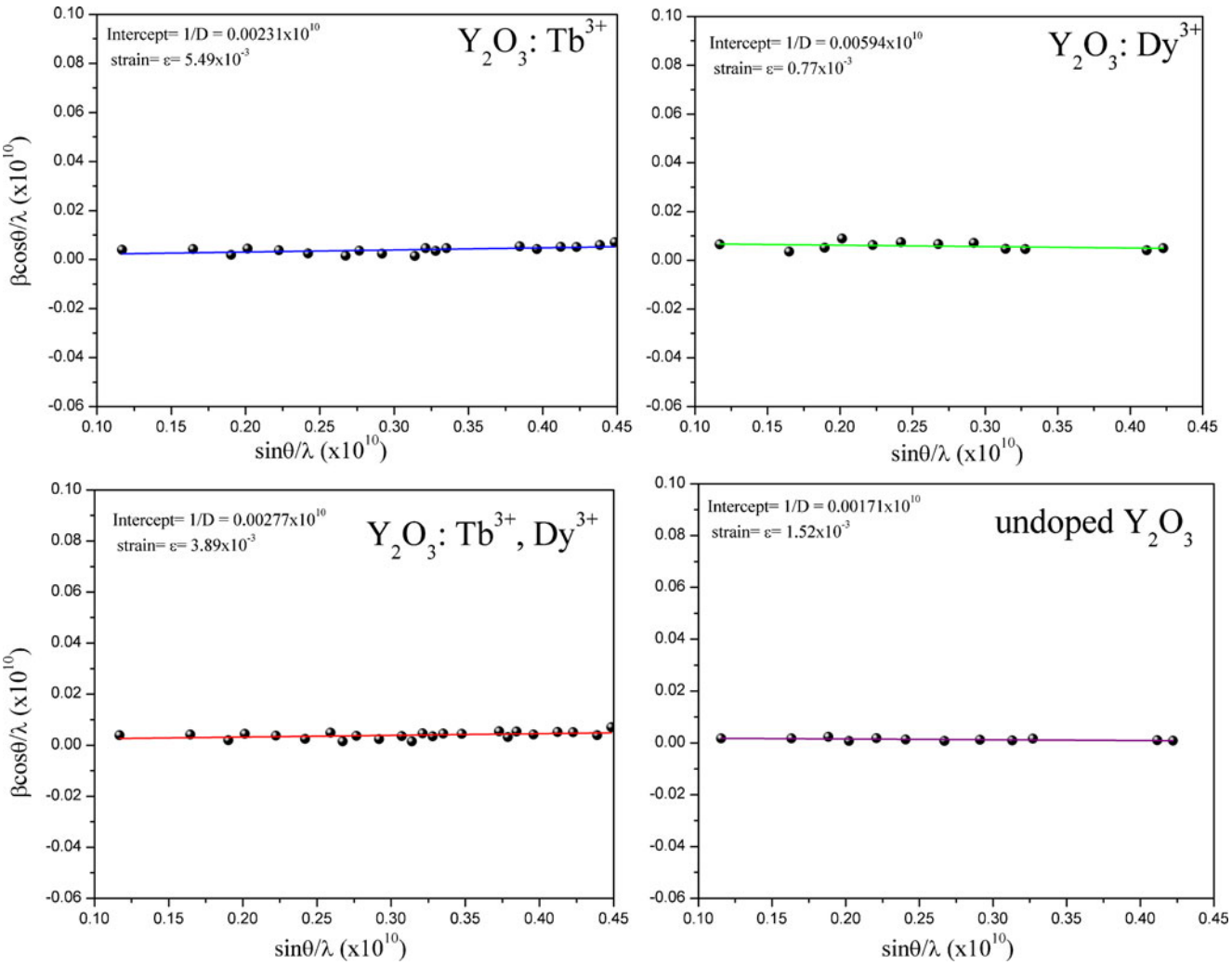

Fig. 2 Hall Williamson plot to calculate the crystallite size

attributed to Y-O lattice vibration. The peaks at 850 cm^{-1} and the ones at 1,060, 1,395 and 1,542 cm^{-1} are due to C-O bond bending and C-O bond stretching vibration respectively. The broad band at 3,550 cm^{-1} is assigned to O-H stretching vibration [16]. This absorption band in the prepared doped samples were probably due to the adsorbed molecular water from KBr pellet technique for FTIR measurements, or the residual carbonate or absorption of H_2O and CO_2 from the ambient atmosphere. The absorption bands due to C-O and O-H vibrations are very weak in the commercial undoped Y_2O_3 phosphor.

The presence of residual hydroxyl group (−OH) in luminescent materials may induce the quenching of the rare earth emission which further reduces the luminescence efficiency. To overcome this problem, the samples were undergone for further heat treatment. Figure 3b–d show the FTIR spectra of Y_2O_3:Tb^{3+}, Y_2O_3:Dy^{3+} and Y_2O_3:Tb^{3+}/Dy^{3+} phosphors annealed at three different temperatures. The FTIR spectra show that the hydroxyl group (−OH) becomes weaker with the increase of annealing temperature and totally disappears at a higher annealing temperature for all the three cases. The decrease in C-O bond vibration with annealing temperature indicates the reduction in carbon content of annealed samples.

Optical Properties

Diffuse Reflectance

The diffuse reflectance spectra of doped and codoped Y_2O_3 powder phosphors were measured against a reference $BaSO_4$ sample. A sharp band at 210 nm was observed in all the samples (Fig. 4) implying that light having this particular wavelength was absorbed. This band was due to

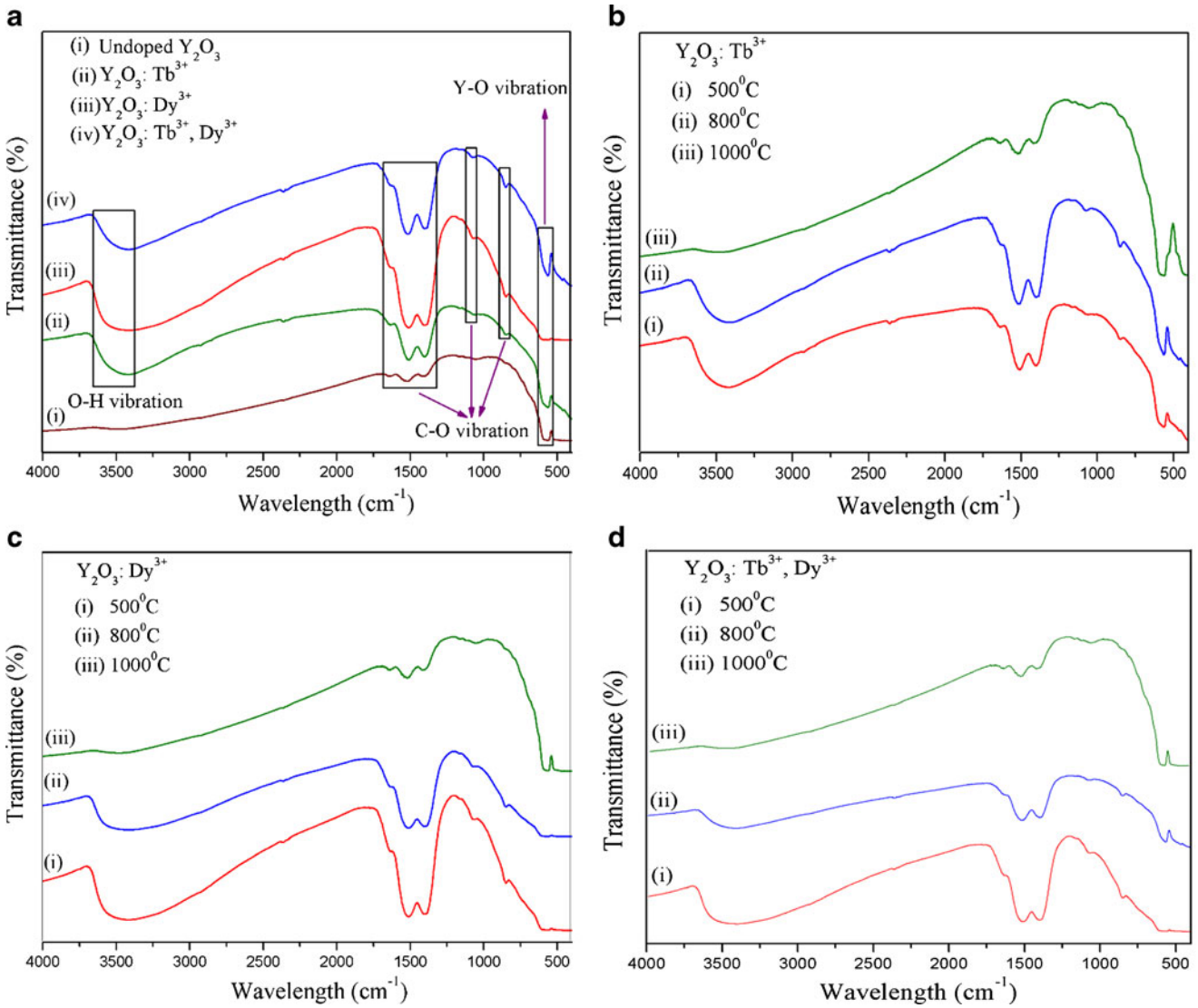

Fig. 3 FT-IR spectra of the prepared samples for different dopants (**a**) and annealing temperature (**b**–**d**)

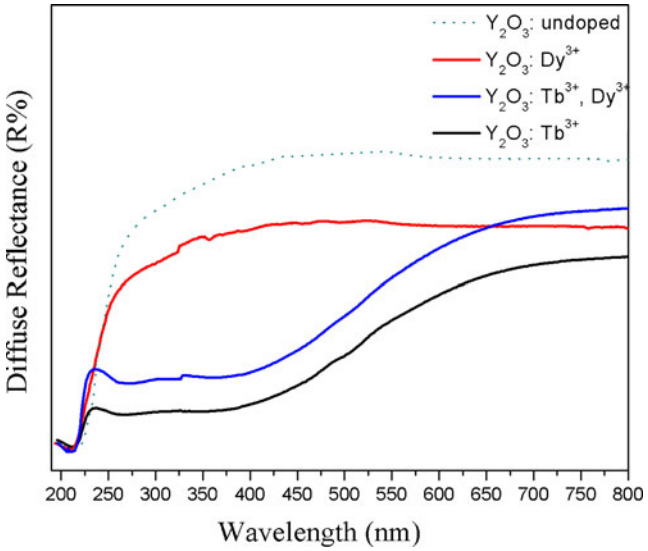

Fig. 4 DR spectra of the prepared samples

band gap of these phosphors. The other bands observed in the spectra were due to meta-stable energy states formed between valence band and conduction band by the doping ions. The absorption edge in case of prepared nanophosphors is shifted towards blue region with respect to undoped sample due to the difference in crystallite size. Among the prepared doped and codoped nanophosphors, the Y_2O_3: Dy^{3+} has the highest diffuse reflectivity.

Calculation of Bandgap

The Kubelka-Munk theory [11] was used to calculate the band gap of doped and codoped Y_2O_3 nanophosphors using diffuse reflectance spectrum. In a diffuse reflectance spectrum, the ratio of the light scattered from a thick layer of sample and an ideal non-absorbing reference sample is measured as a function of the wavelength λ, $R_\infty = R_{sample}/R_{reference}$ [17]. The relation between the diffuse reflectance of the sample (R_∞),

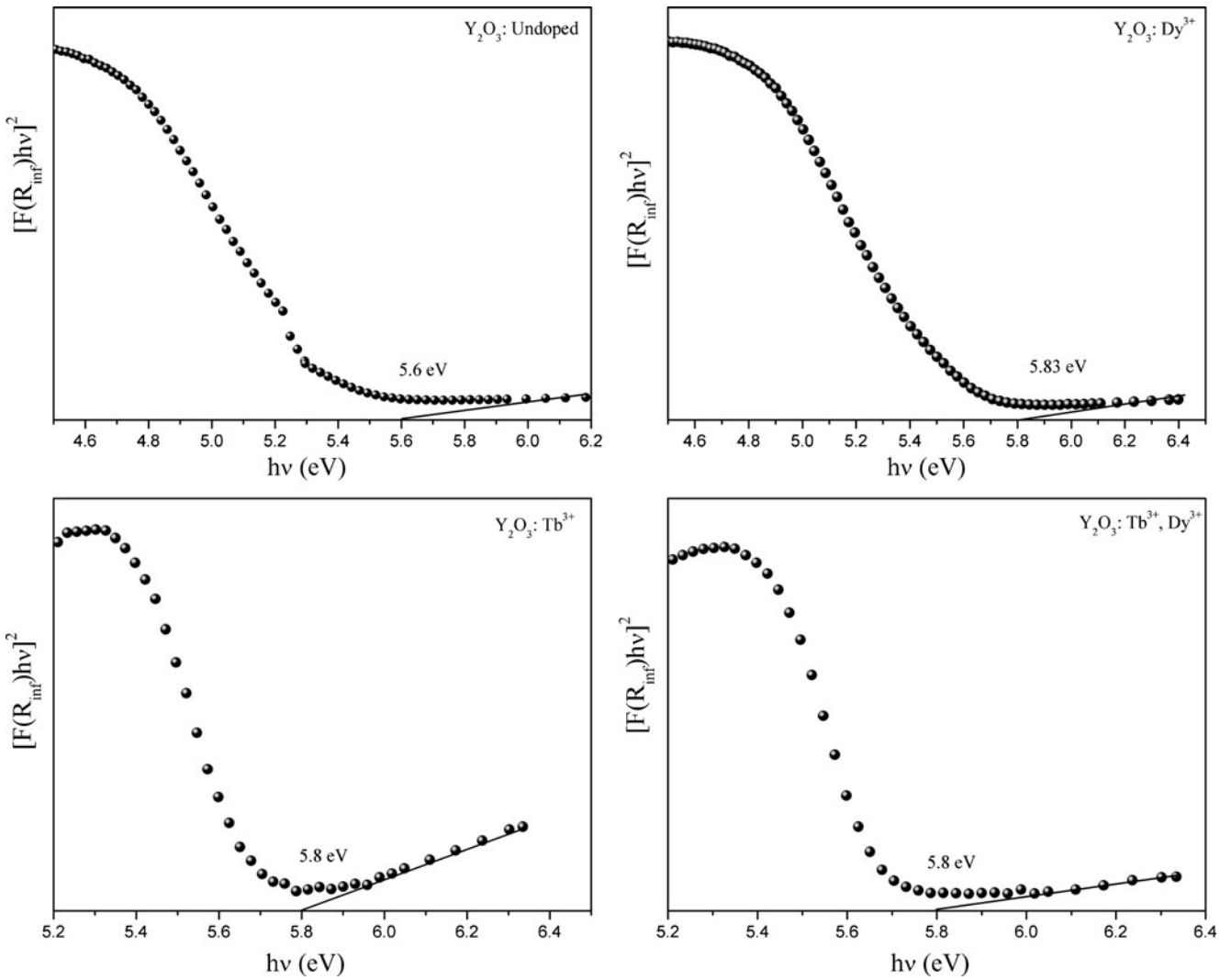

Fig. 5 Bandgap calculation of the prepared samples

absorption coefficient (K) and scattering coefficient (S) is given by the Kubelka-Munk function $F(R_\infty)$:

$$F(R_\infty) = \frac{(1 - R_\infty)^2}{2R_\infty} = \frac{K}{S} \quad (5)$$

The band gap E_g and absorption coefficient α of a direct band gap semiconductor is related through the well-known Tauc relation:

$$\alpha h\nu = C_1 \left(h\nu - E_g\right)^{1/2} \quad (6)$$

where α is the linear absorption coefficient, ν is the photon energy and C_1 is a proportionality constant. When the material scatters in perfectly diffuse manner (or when it is illuminated at 60° incidence), the absorption coefficient K becomes equal to 2α. Considering the scattering coefficient S as constant with respect to wavelength, and using Eqs. 5 and 6, the following expression can be written:

$$[F(R_\infty)h\nu]^2 = C_2\left(h\nu - E_g\right) \quad (7)$$

From the plot of $[F(R_\infty)h\nu]^2$ versus $h\nu$, the value of E_g was obtained by extrapolating the linear fitted regions to $[F(R_\infty)h\nu]^2=0$. The curve of Fig. 5 exhibits nonlinear and linear portions, which is the characteristic of direct allowed transition. The nonlinear portion corresponds to a residual absorption involving impurity states and linear portion characterizes the fundamental absorption.

The calculated band gap is summarized in Table 2. The difference in the band gap of phosphors is due to difference in the crystallite size, smaller the crystallite size greater is the band gap.

Influence of Doping Concentration on Photoluminescence

The performance of luminescent materials can be improved by changing the doping concentration and it is very important factor to determine the optimum concentration of dopant. Photoluminescence spectra of Y_2O_3:Dy^{3+} and Y_2O_3:Tb^{3+} phosphors for different concentrations (0.1 mol%–5 mol%) of Dy^{3+} and Tb^{3+} ions are shown in Fig. 6a and b. The excitation wavelengths for the two phosphors were kept at 351 and 275 nm respectively.

The emission spectra of Y_2O_3: Dy^{3+} consists of two distinct peaks at 488 and 575 nm corresponding to the $^4F_{9/2} \rightarrow {}^6H_{15/2}$ and $^6H_{13/2}$ transitions respectively (Fig. 6a). The 351 nm radiation excites the Dy^{3+} ions to the $^6P_{7/2}$ level and then quickly relaxes to $^4F_{9/2}$ level by emitting nonradiative transitions. The strong yellow emission band centered at 575 nm corresponds to the

Table 2 Optical parameters of doped and codoped Y_2O_3 phosphors

Phosphor	Bandgap (eV)	Transition	Wavelength (nm)	Concentration/Mass ratio	Colour ratio
Y_2O_3: Dy^{3+}	5.83	**$^4F_{9/2} \rightarrow {}^6H_{13/2}$ (most Intense)**	**575**	0.1	0.79 (B/Y)
				0.5	0.79(B/Y)
		$^4F_{9/2} \rightarrow {}^6H_{15/2}$	488	1	0.78(B/Y)
				2	0.76(B/Y)
				5	0.79(B/Y)
Y_2O_3: Tb^{3+}	5.8	$^5D_4 \rightarrow {}^7F_3$	625	0.1	0.52 (B/G)
		$^5D_4 \rightarrow {}^7F_4$	585	0.5	0.47(B/G)
		$^5D_4 \rightarrow {}^7F_5$ (most Intense)	**542**	1	0.42(B/G)
					0.46(B/G)
		$^5D_4 \rightarrow {}^7F_6$	485	2	0.56(B/G)
Y_2O_3: Dy^{3+}, Tb^{3+}	5.8	**$^4F_{9/2} \rightarrow {}^6H_{13/2}$(Intense)**	**575**	1:1	0.45 (G/Y)
		$^4F_{9/2} \rightarrow {}^6H_{15/2}$	488	1:2	0.47(G/Y)
		$^5D_4 \rightarrow {}^7F_3$	625	1:4	0.64(G/Y)
		$^5D_4 \rightarrow {}^7F_4$	585	1:6	0.85(G/Y)
		$^5D_4 \rightarrow {}^7F_5$ (Intense)	**542**	1:8	0.82(G/Y)
		$^5D_4 \rightarrow {}^7F_6$	485	1:1	0.35 (B/Y)
				1:2	0.33 (B/Y)
				1:4	0.32 (B/Y)
				1:6	0.28 (B/Y)
				1:8	0.27 (B/Y)
Undoped Y_2O_3	5.6	-	-	-	-

B=Blue, **Y**=Yellow, **G**=Green

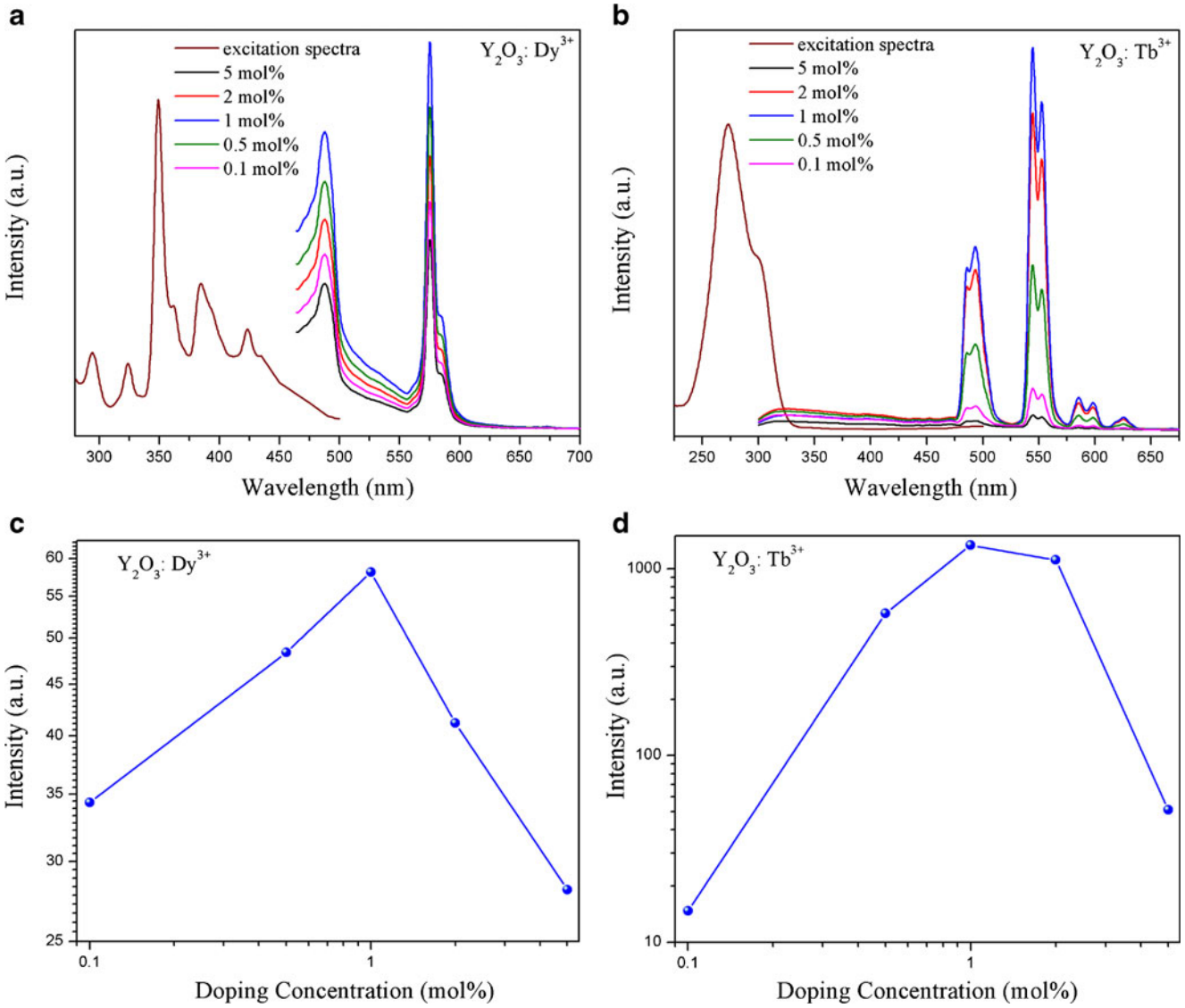

Fig. 6 PL emission and excitation spectra of Dy^{3+} doped (**a**), Tb^{3+} doped (**b**) Y_2O_3 phosphors at different doping concentrations

hypersensitive transition $^4F_{9/2} \rightarrow {}^6H_{13/2}$. Another feeble blue emission band at 488 nm corresponds to the $^4F_{9/2} \rightarrow {}^6H_{15/2}$ transition, which is less sensitive to the host. The emission intensity increases with increase in the Dy^{3+} concentration upto 1 mol% and then decreases when the concentration is >1 mol% due to quenching phenomena (Fig. 6c).

The reason behind observing the intense yellow emission from Y_2O_3: Dy^{3+} can be understood by considering the structure of Y_2O_3. The coordination number of Y_2O_3 is six and forms cubic bixbyite structure with two different sites (C_2 and C_{3i}) for RE^{3+} ions substitution (Fig. 7). Y^{3+} ions in unit cell occupy 24 sites with point symmetry C_2 and 8 sites with point symmetry C_{3i} (i.e. totally 32 sites that comprise the unit cell of Y_2O_3). The C_2 is a low symmetry site without an inversion center whereas C_{3i} is a high symmetry site having an inversion center. When Dy^{3+} is located at a low symmetry (C_2), the yellow emission is dominant whereas the blue emission is dominant when Dy^{3+} is located at a high symmetry (C_{3i}) [8]. In the present case, yellow emission at 575 nm ($^4F_{9/2} \rightarrow {}^6H_{13/2}$) is dominant suggesting that the location of Dy^{3+} is more favourable at C_2 site. As the C_2 site does not have an inversion center, electric dipole transitions from Dy^{3+} ions attached to this site are more favourable than the magnetic dipole transitions. So, the intense yellow emission from Dy^{3+} around 575 nm is of electric dipole and feeble blue emission around 488 nm is of magnetic dipole origin. The similarity of the ionic radii of Dy^{3+} and Y^{3+} ions allows the easy substitution of Y^{3+} ions with Dy^{3+} ions at C_2 sites giving rise to intense yellow emissions in all the samples.

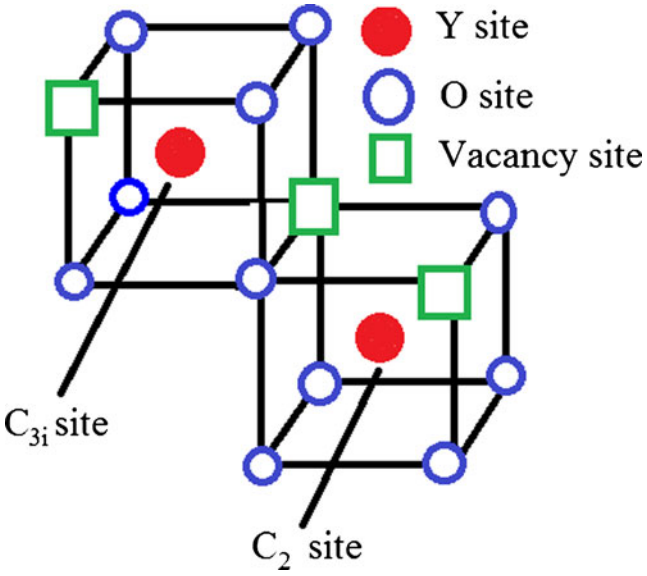

Fig. 7 C_2 and C_{3i} symmetry sites of Y ions in cubic crystals structure of Y_2O_3

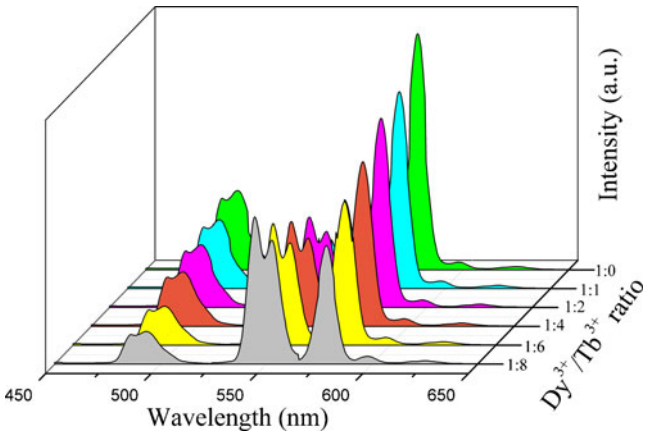

Fig. 9 PL emission spectra of Y_2O_3 phosphor codoped with various mass ratios of Dy^{3+} to Tb^{3+} under 351 nm excitation

The excitation spectrum of 1 mole% Dy doped Y_2O_3 was recorded keeping the emission wavelength at 575 nm (Fig. 6a). This spectra consists of several excitation bands of f-f transitions, which are ascribed to the different transitions from the ground state $^6H_{15/2}$ to the various excited

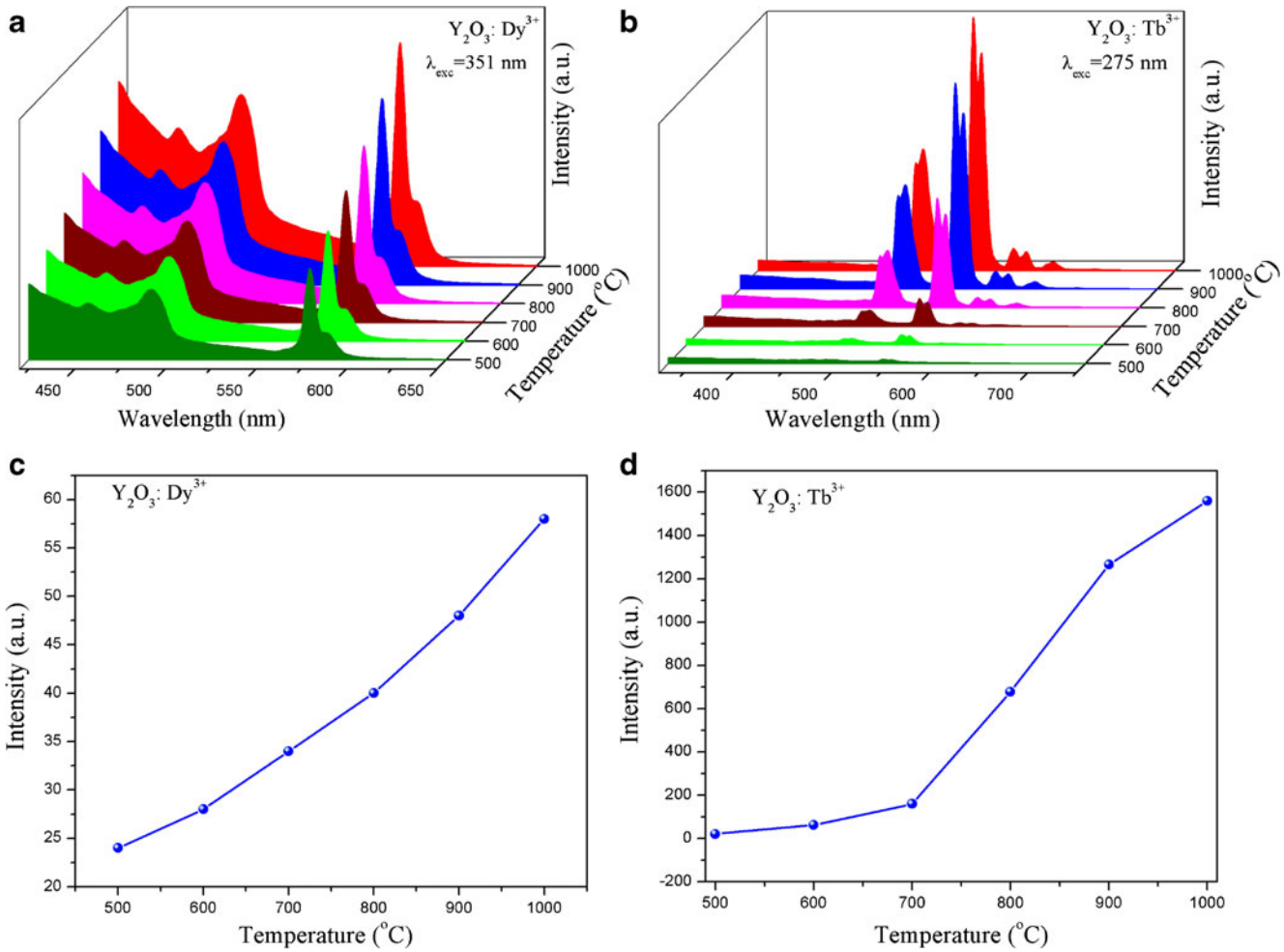

Fig. 8 PL emission and excitation spectra of Dy^{3+} doped (**a**), Tb^{3+} doped (**b**) Y_2O_3 phosphors at different annealing temperatures

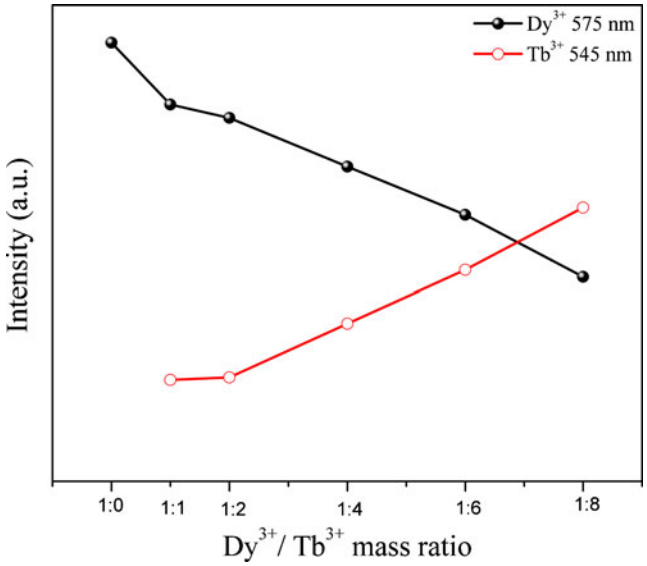

Fig. 10 Integrated intensity of Dy^{3+} 575 nm and Tb^{3+} 545 nm as function of various mass ratios of Dy^{3+} to Tb^{3+} ions

states of $4f^9$ electronic configuration of the Dy^{3+} ions. The excitation maxima located at 351 nm corresponds to the hypersensitive transition from the ground $^6H_{15/2}$ to $^6P_{7/2}$ level [18].

The emission spectra of Y_2O_3: Tb^{3+} (Fig. 6b) is composed of several distinct peaks at 485, 542, 585 and 625 nm corresponding to the $^5D_4 \rightarrow {}^7F_J$ transitions (J=3, 4, 5 and 6). The strongest transition at 542 nm corresponding to $^5D_4 \rightarrow {}^7F_5$ transition is due to green emission of Tb^{3+} [19]. The other peaks at 485 nm, 585 nm and 625 nm arose from the $^5D_4 \rightarrow {}^7F_6$, $^5D_4 \rightarrow {}^7F_4$ and $^5D_4 \rightarrow {}^7F_3$ transitions respectively. The Tb^{3+} concentration was varied from 0.1 mol% to 5 mol% and it was observed that the intensity increases upto 1 mol% and then decreases concluding that the optimum doping concentration of Tb^{3+} in Y_2O_3 host is 1 mol% (Fig. 6d). The decrease in PL intensity of phosphors for concentration of Tb^{3+} greater than 1 mol% may have been caused by cross-relaxation between neighbouring Tb^{3+} ions resulting in the quenching phenomena.

The excitation spectrum of 1 mol% Tb^{3+} doped Y_2O_3 was recorded keeping the emission wavelength fixed at 542 nm (Fig. 6b). Two overlapping bands at 275 and 302 nm were observed due to f–d transitions [20]. However, because of parity forbiddenness of the transition within 4f configuration the peaks in the excitation spectra beyond 302 nm are too weak to observe here.

Influence of Annealing Temperature on Photoluminescence

Figure 8a and b shows the photoluminescence emission spectra of the Y_2O_3:Dy^{3+} and Y_2O_3:Tb^{3+} phosphors annealed at different temperatures 500 °C to 1,000 °C. Here the optimum concentration (1 mol%) of Tb^{3+} and Dy^{3+} were taken. The emission intensity increases with the increase of annealing temperature. Above 700 °C, the emission intensity increases significantly due to increased growth in the crystallinity and good dispersion of doping components inside the host material confirming the results obtained from the XRD.

The integrated intensity of yellow emission from the Y_2O_3: Dy^{3+} annealed at 1,000 °C is ~2.5 times higher than that of the sample annealed at 500 °C whereas the intensity

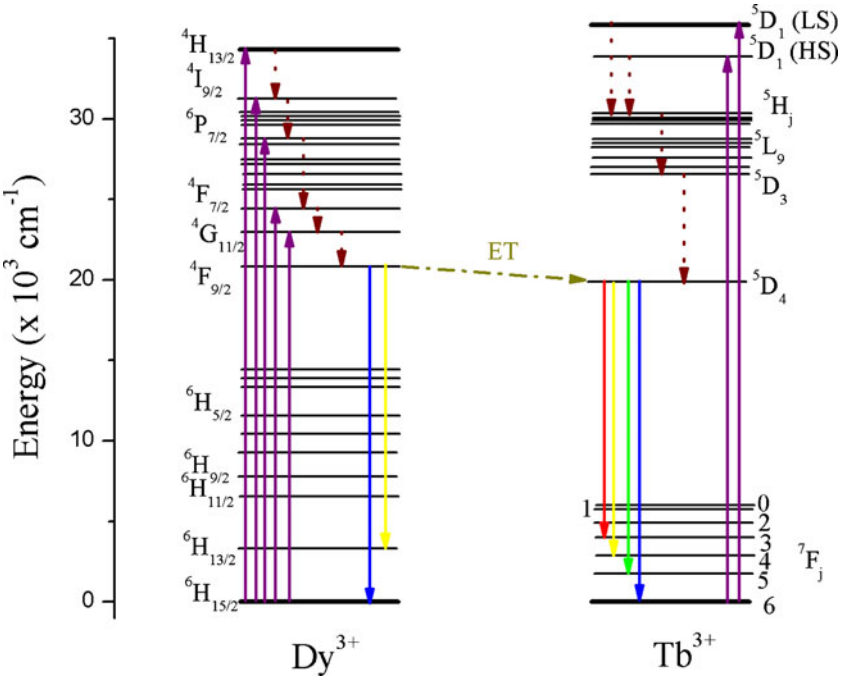

Fig. 11 Energy level diagrams and energy transfer phenomena between Dy^{3+} and Tb^{3+}

of green emission from Y_2O_3: Tb^{3+} increases ~25 times for the same temperature rise. Moreover, blue to yellow (B/Y) intensity ratio (I_{488}/I_{575}) for all the annealed Y_2O_3: Dy^{3+} samples comes out to be 0.76–0.79 whereas blue to green (B/G) intensity ratio (I_{485}/I_{542}) for all the annealed Y_2O_3: Tb^{3+} samples comes out to be 0.42–0.56. The values are summarized in Table 2. As the B/Y ratio is approximately constant for Y_2O_3: Dy^{3+} annealed phosphors and hence pure white light emission from this phosphor can be achieved by tailoring this B/Y ratio via codoping with other rare earth ions Tb^{3+} [8].

Influence of Codoping on Photoluminescence

Figure 9 shows the photoluminescence emission spectra of $(Y_{1-x-y}Dy_xTb_y)_2\ O_3$ with taking the mass ratio Dy/Tb as 1:0, 1:1, 1:2, 1:4, 1:6, 1:8 under 351 nm excitation. The obtained data is summarized in Table 2. The intensity of green emission from Tb^{3+} was enhanced by codoping with Dy^{3+} ions and the corresponding integrated intensities of Dy^{3+} 575 nm and Tb^{3+} 542 nm are also illustrated in Fig. 10., which indicates that energy transfer occurred from Dy^{3+} to Tb^{3+} ions [5].

Figure 11 describes the energy level diagrams of Dy^{3+} and Tb^{3+}, showing the radiative and nonradiative transitions and also the energy transfer from Dy^{3+} to Tb^{3+} ions [18]. When the 4f higher energy level of Dy^{3+} is excited with 351 nm wavelength light, the initial population relaxes to lower energy levels until it arrives at the $^4F_{9/2}$ level by phonon assistance. With the emission of phonons, part of the energy from the $^4F_{9/2}$ level of Dy^{3+} is transferred to the $^5D_4$ level of Tb^{3+} by dipole–dipole interaction between the two energy levels, resulting in the enhancement of Tb^{3+} 542 nm emission.

Conclusions

The XRD studies of doped and codoped phosphors indicates that the introduction of Tb^{3+},Dy^{3+} ions do not influence the crystal structure of the phosphor. The crystallinity and crystallite size phosphors improve with an increase in annealing temperature. In the FTIR spectra, absorption bands were observed corresponding to Y-O, C-O and O-H vibrations. The FTIR studies show that the hydroxyl group (−OH) in prepared phosphors becomes weaker with the increase of annealing temperature causing the increase in luminescence efficiency. The bandgap of the phosphors from DRS were found to be of the order of 5.8 eV. Due to wide bandgap, these phosphors can be used as the promising candidate for applications in different optoelectronic devices. Photoluminescence studies confirm that the Dy^{3+} ions mostly replace the Y^{3+} ions of C_2 site in Y_2O_3 lattice. The blue to yellow (B/Y) intensity ratio (I_{488}/I_{575}) of Y_2O_3: Dy^{3+} phosphor and the blue to green (B/G) intensity ratio (I_{485}/I_{542}) of Y_2O_3: Tb^{3+} phosphor was found to be almost constant over the whole range of doping concentration and annealing temperatures. The pure white light emission from doped Y_2O_3 phosphor can be achieved by tailoring the two intensity ratios via codoping which causes the enhancement of the Tb^{3+} emission as a result of non-radiative energy transfer from Dy^{3+} to Tb^{3+} in Yttrium oxide host.

Acknowledgements The authors are thankful to University Grants Commission, New Delhi, Government of India for funding this work (Project F. No. 37-200/2009 (SR)).

References

1. Cho SH, Kwon SH, Yoo JS, Oh CW, Lee JD, Hong KJ, Kwon SJ (2000) Cathodoluminescent characteristics of a spherical Y_2O_3: Eu phosphor screen for field emission display application. J Electrochem Soc 147:3143–3147
2. Martinez-Rubio MI, Ireland TG, Fern GR, Silver J, Snowden MJ (2001) A New Application for Microgels: Novel Method for the Synthesis of Spherical Particles of the Y_2O_3: Eu Phosphor Using a Copolymer Microgel of NIPAM and Acrylic Acid. Langmuir 17:7145–7149. doi:10.1021/la0105883
3. Chien Wen-Chen Y, Yang-Yen YC-C (2010) A novel synthetic route to Y_2O_3:Tb^{3+} phosphors by bicontinuous cubic phase process. Mater Des 31:1737–1741. doi:10.1016/j.matdes.2009.01.046
4. Singh LR, Ningthoujam RS, Sudarsan V, Srivastav I, Singh SD, Dey GK, Kulshreshtha SK (2008) Luminescence Study of Eu^{3+} doped Y_2O_3 Nanoparticles: Particle Size, Concentration and core-Shell Formation Effects. Nanotechnology 19:055201–8. doi:10.1088/0957-4484/19/05/055201
5. Xin-Yuan S, Gua M, Shi-Ming H, Xiao-Lin L, Bo L, Chen N (2009) Enhancement of Tb^{3+} emission by non-radiative energy transfer from Dy^{3+} in silicate glass. Physica B 404:111–114. doi:10.1016/j.physb.2008.10.039
6. Maruyama N, Honma T, Komatsu T (2009) Enhanced quantum yield of yellow photoluminescence of Dy^{3+} ions in nonlinear optical $Ba_2TiSi_2O_8$ nanocrystals formed in glass. Journal of Solid State Chemistry 182(2):246–252. doi:10.1016/j.jssc.2008.10.028
7. Kharabe VR, Dhoble SJ, Moharil SV (2008) Synthesis of Dy^{3+} and Ce^{3+} activated $Sr_6BP_5O_{20}$ and $Ca_6BP_5O_{20}$ borophosphate phosphors. J Phys D Appl Phys 41:205413. doi:10.1088/0022-3727/41/20/205413
8. Jayasimhadri M, Moorthy LR, Kojima K, Yamamoto K, Wada N, Wada N (2006) Optical properties of Dy^{3+} ions in alkali Tellurophosphate glasses for laser materials. J Phys D Appl Phys 39:635–641. doi:10.1088/0022-3727/39/4/007
9. Qingyu M, Chen Baojiu XW, Yanmin Y, Xiaoxia Z, Di Weihua L, Shaozhe WX, Jiashi S, Cheng Lihong Y, Tao PY (2007) Size-dependent excitation spectra and energy transfer in Tb^{3+}-doped Y_2O_3 nanocrystalline. J Appl Phys 102:093505–6. doi:10.1063/1.2803502
10. Nash Kelly L, Dennis Robert C, Gruber John B, Sardar Dhiraj K (2009) Intensity analysis and energy-level modeling of Nd^{3+} in Nd^{3+}:Y_2O_3 nanocrystals in polymeric hosts. J Appl Phys 105:033102–6. doi:10.1063/1.3074313

11. Morales AE, Mora ES, Pal U (2007) Use of diffuse reflectance spectroscopy for optical characterization of un-supported nanostructures. Revista Mexicana de F´isica S 53(5):18–22
12. Vu N, Anh TK, Yi G, Strek W (2007) Photoluminescence and cathodoluminescence properties of Y_2O_3: Eu nanophosphors prepared by combustion synthesis. J Lumin 122–123:776–779. doi:10.1016/j.lumin.2006.01.286
13. Chatterjee SK (2010) X-Ray Diffraction Its Theory and Applications. PHI Learning Private Ltd. 2nd Edn.: 92–98.
14. Yen-Pei F (2007) Preparation and characterization of Y2O3:Eu phosphors by combustion process. J Mater Sci 42:5165–5169. doi:10.1007/s10853-006-1289-8
15. Vij A, Kumar R, Chawla AK, Lochab SP, Chandra R, Singh N (2010) Swift heavy ion induced synthesis and enhanced photoluminescence of SrS: Ce nanoparticles. Opt Mater 33:58–62. doi:10.1016/j.optmat.2010.07.024
16. Wang C, Zhao J, Yong LI, Zhang W, Yin M (2009) Influence of dispersant on Y_2O_3: Eu^{3+} powders synthesized by combustion method. Journal of Rare Earths 27(6):879–885. doi:10.1016/S1002-0721(08)60354-3
17. Rao G R, Sahu H R (2001) XRD and UV–vis diffuse reflectance analysis of CeO_2– ZrO_2 solid solutions synthesized by combustion method. Proc. Indian Acad. Sci. (Chem. Sci.), 113: 651.
18. Gao D, Li Y, Lai X, Wei Y, Bi J, Li Y, Liu M (2011) Fabrication and Luminescence properties of Dy^{3+} doped $CaMoO_4$ powders. Material Chemistry and Physics 126:391–397. doi:10.1016/j.matchemphys.2010.10.053
19. Liu Zhilong Y, Lianxiang WQ, Yanchun T, Hua Y (2011) Effect of Eu, Tb codoping on the luminescent properties of Y2O3 nanorods. J Lumin 131:12–16. doi:10.1016/j.jlumin.2010.08.012
20. Pitale SS, Sharma SK, Dubey RN, Qureshi MS, Malik MM (2009) Luminescence behavior of SrS:Pr^{3+} micron-sized phosphor fabricated through chemical co-precipitation route and post-annealing processes. Opt Mater 31:923–930. doi:10.1016/j.optmat.2008.10.048